Wiley
Journal of Food Biochemistry
Volume 2025, Article ID 8616106, 11 pages
https://doi.org/10.1155/jfbc/8616106

WILEY

Research Article

Chemical Characterization of *Rheum tanguticum* Petiole Juice via Membrane Filtration: A Comparative Analysis Using UPLC–QTOF–MS–MS and Network Pharmacology

Chen Chen,[1,2] **Zengrong Ye**,[3] **Jianan Li**,[2] **Na Liu**,[2] **Bo Wang**,[2] **and Guoying Zhou**[2]

[1]*Anhui Provincial Engineering Laboratory for Efficient Utilization of Featured Resource Plants, College of Life Sciences, Huaibei Normal University, Huaibei, Anhui 235000, China*
[2]*Northwest Institute of Plateau Biology, Chinese Academy of Sciences Key Laboratory of Tibetan Medicine Research, Xining 810008, China*
[3]*Qinghai University, Xining 810000, China*

Correspondence should be addressed to Guoying Zhou; zhougy@nwipb.cas.cn

Received 2 April 2024; Revised 9 April 2024; Accepted 7 August 2025

Academic Editor: Hassan Ahmadi Gavlighi

Copyright © 2025 Chen Chen et al. Journal of Food Biochemistry published by John Wiley & Sons Ltd. This is an open access article under the terms of the Creative Commons Attribution License, which permits use, distribution and reproduction in any medium, provided the original work is properly cited.

Rheum tanguticum petiole juice, widely consumed in Tibet as both a vegetable and an herb, exhibits varying chemical compositions depending on the production methods. This study aims to identify the bioactive components in raw juice using ultra-performance liquid chromatography–quadrupole time-of-flight tandem mass spectrometry (UPLC–QTOF–MS–MS) and analyze their antidiabetic properties through network pharmacology. In addition, the effects of the three types of membrane clarification were evaluated. A total of 36 compounds were identified, and a components–targets–pathways–disease network was constructed for diabetes treatment. Among the membranes tested, the 0.2 μm microfiltration membrane exhibited the highest permeate flux and retained significant amounts of total flavonoids, phenolics, and proanthocyanidins, making it the optimal choice for juice clarification. These findings lay the groundwork for the industrial processing and utilization of *R. tanguticum* petiole juice in China.

Keywords: membrane separation; network pharmacology; petioles juice; UPLC–QTOF–MS–MS

1. Introduction

Rhubarb, an herb from the Polygonaceae family, is globally recognized and includes over 60 varieties. It is predominantly found in Asia, with China serving as the central hub. Rhubarb has a rich medicinal history, first documented in the "Shennong Materia Medica," and is known for treating diarrhea, reducing heat and inflammation, cooling blood, detoxifying, resolving stasis, promoting menstruation, and alleviating dampness [1]. Recent studies have expanded our understanding of rhubarb's pharmacological activities, revealing its purgative, antitumor, anti-inflammatory, analgesic, and antioxidant properties, as well as its ability to protect the liver and gallbladder, and combat microbial infections [2–4].

Rhubarb petioles are used as vegetables in various regions, offering diverse health benefits [5–7]. In Europe and the United States, rhubarb petioles are incorporated into vegetable salads, canning, jams, jellies, sauces, and ciders [8]. In Turkey, locals consume fresh rhubarb petioles as vegetables and use them in appetizers. *Rheum tanguticum* (RT) Maxim. ex Regel, a type of rhubarb, is one of the oldest and most significant traditional Tibetan medicines. The petioles of this species are known for their sour taste and potential antidiabetic properties. Traditionally, Tibetans squeeze the petioles of RT to make juice for both people and animals in the Tibet region.

With the advancement of the national strategy for traditional Chinese medicine, numerous RT cultivation bases have been established in Gansu and Qinghai, covering nearly 300,000 ha. Efficient use of RT petioles is crucial; failure to do so could lead to significant waste of biological resources and environmental pollution from decomposition. Despite this, the production of RT petiole juice on a semi-industrial scale remains limited locally. Traditional petiole juice production relies primarily on crushing methods, and there is a notable lack of information regarding industrial-scale processing and the composition of petiole.

Membrane processes such as ultrafiltration (UF), microfiltration (MF), and reverse osmosis (RO) are gaining popularity for juice clarification and concentration in the fruit juice sector. These membrane processes offer several advantages over conventional production methods, including lower energy consumption, higher efficiency, and the absence of chemical agents or phase changes [9]. MF and UF, in particular, have been effectively used for clarifying and concentrating various types of fruit juices, including passion fruit, purple, pequi, and mulberry juices [10–13]. This suggests potential applicability in the processing of RT petiole juice.

Currently, there is no standardized method for processing RT petiole juice using membrane technology. Furthermore, the existing literature provides limited information on the bioactive compounds present in RT petiole juice and their interactions with various biological targets. This study aims to address these gaps by (1) identifying the bioactive compounds in raw RT petiole juice through ultra-performance liquid chromatography–quadrupole time-of-flight tandem mass spectrometry (UPLC–QTOF–MS–MS), (2) utilizing network pharmacology to explore the molecular mechanisms of these compounds in diabetes, and (3) assessing the physicochemical properties of the juice after applying MF and UF technologies. The findings from this research could pave the way for the development of RT petiole juice as a nutritious food source and its application in industrial processing.

2. Materials and Methods

2.1. Reagents. MS grade formic acid and acetonitrile were purchased from Merck (Germany). Gallic acid was obtained from Macklin (China). Sodium carbonate (Na_2CO_3), Coomassie Brilliant Blue G–250, sodium nitrite ($NaNO_2$), hydrogen peroxide (H_2O_2), aluminum nitrate ($Al(NO_3)_3$), sodium hydroxide (NaOH), sulfuric acid (H_2SO_4), nitric acid (HNO_3), and hydrochloric acid (HCl) were procured from Sinopharm Chemical Reagent Co., Ltd (China). Standard solutions of calcium (Ca), aluminum (Al), iron (Fe), magnesium (Mg), potassium (K), manganese (Mn), sodium (Na), and zinc (Zn) were sourced from Aladdin (China).

2.2. Materials. Fresh petioles of RT were collected from a planting base in Huzhu County, Qinghai Province, China (36° 50′ 15″N, 101° 57′ 07″E, 3050 m) in August 2023. The fresh petioles were cleaned with tap water, and the raw juice was extracted using a hydraulic press. The fresh raw juice was stored at 4°C before use. Prior to membrane filtration and content determination, the raw juice underwent preliminary filtration using gauze to eliminate solid residues.

2.3. Chemical Composition of the Raw Petiole Juice. To identify secondary metabolites in fresh petiole juice, we utilized the 6546 Series UPLC–QTOF–MS–MS system (Agilent, USA). The analysis employed a Zorbax C_{18} column (150 × 2.1 mm i.d.; 5 μm) with a stepwise gradient mode consisting of 0.1% formic acid (Solvent A) and acetonitrile (Solvent B) at a temperature of 35°C and a flow rate of 0.3 mL/min. The elution process began with a linear gradient of Solvent B, increasing from 5% to 45% in 35 min. Mass spectrometry parameters were set as follows: the mass range ranged from 100 to 1500 m/z in the negative ion mode. The atomizing gas was set at 53 psi, while the curtain air was maintained at 34 psi. The ion source temperature was held at 550°C, and the ion source voltage was set at 4500 V.

2.4. Network Pharmacology Construction. Initially, the active compounds present in the raw petiole juice were identified using UPLC–QTOF–MS–MS. The 36 compounds were selected based on absorption, distribution, metabolism, and excretion (ADME) parameters, with specific screening thresholds of oral bioavailability (OB) > 30% and drug-likeness (DL) > 0.18. Corresponding molecular structures were retrieved from the PubChem database.

Potential antidiabetic targets were systematically retrieved from three authoritative databases using standardized protocols. Initial screening was performed using "diabetes" as the primary search term across: (1) GeneCards, retaining only human genes with relevance scores ≥ 12; (2) NCBI Gene database with species filter for Homo sapiens; and (3) DisGeNET, applying a stringent score cutoff ≥ 0.02 for gene–disease associations. The resulting gene lists were merged, and duplicate entries were removed to generate a comprehensive set of diabetes-related targets.

The diabetes-related target genes were analyzed using the STRING database with the following parameters: (1) species restriction to Homo sapiens, (2) minimum interaction score threshold > 0.4, and (3) removal of isolated protein nodes. This generated a protein–protein interaction (PPI) network, representing potential therapeutic targets for diabetes. The network data were exported in TSV format and subsequently imported into Cytoscape for topological analysis. NetworkAnalyzer was employed to calculate six key centrality parameters for each node: betweenness centrality (BC), closeness centrality (CC), degree centrality (DC), eigenvector centrality (EC), network centrality (NC), and local average connectivity (LAC). Nodes with higher values for these parameters were considered more biologically significant within the network architecture.

Gene Ontology (GO) and Kyoto Encyclopedia of Genes and Genomes (KEGG) pathway enrichment analyses were performed on the core targets derived from the analysis of PPI networks using the Database for Annotation,

Visualization, and Integrated Discovery (DAVID) database. Finally, the DAVID database was utilized for annotation and to identify the enriched pathways of the core targets.

2.5. MF of Juice. Filtration experiments were conducted using a membrane separation apparatus supplied by Shijie Corporation (Hefei, China). The setup comprised a centrifugal pump, a 25 L feed tank, a cooling tank with tap water, and a pressure regulating valve. Polyvinylidene fluoride (PVDF) membranes with pore sizes of 0.1 and 0.2 μm for MF and with a molecular weight cutoff (MWCO) of 50 kDa for UF were used. Before juice treatment, all membranes underwent a 24 h conditioning process in pure water before placement in the cell. Following juice treatment, permeate samples were collected, and the membrane equipment was cleaned to restore its original permeability. The permeate flux (Jp) through each membrane, under specific pressure conditions, was determined as the volume permeated per unit area and per unit time, according to the following equation:

$$\mathrm{Jp} = \frac{\mathrm{Vp}}{A * t}, \tag{1}$$

where Vp (L) represents the volume of permeate, A (m^2) stands for the membrane area, and t (h) denotes the operation time. Both the average and relative standard deviation were computed accordingly.

2.6. Analysis of Physicochemical Properties

2.6.1. Determination of Total Phenol Content. The total phenol content was assessed using the modified Folin method, as previously documented with minor adaptations [14]. Gallic acid standard solutions (0.05 mg/mL) were prepared by combining different volumes (0, 0.1, 0.2, 0.3, 0.4, and 0.6 mL) with 1 mL of water in centrifuge tubes. To each tube, 0.5 mL of Folin reagent and 2 mL of 20% Na_2CO_3 solution were successively added, followed by additional water to achieve a final volume of 5 mL. The resulting solution was then incubated in darkness for 40 min at 45°C in a water bath before being assessed using a spectrophotometer (Thermo, USA) set to 760 nm. A standard curve was constructed using concentrations plotted against absorbance values. Samples were detected following a similar procedure to that used for the standard curve determination.

2.6.2. Determination of Soluble Protein. The soluble protein concentration was assessed following the procedure outlined by Zhu et al. [15]. Specifically, 2 mL of the juice was centrifuged at 10,000g for 10 min. After centrifugation, 0.5 mL of the supernatant was combined with 3 mL of Coomassie Brilliant Blue G–250 solution. Following a 2-min incubation period, the absorbance at 595 nm was recorded using a spectrophotometer reader (Thermo, USA).

2.6.3. Determination of Trace Element Content. The trace element content was determined using the ICP–OES method as previously documented [16]. Samples were analyzed for elemental composition using the Optima 8000 ICP–OES system (PerkinElmer, USA), with the following primary conditions: RF power set to 1300 W, nebulizer gas flow at 1.2 L/min, auxiliary gas flow at 0.2 L/min, and sample uptake rate at 1.0 L/min. Initially, 0.2 g of the sample was mixed with 8 mL of HNO_3 and 2 mL of H_2O_2 in a polytetrafluoroethylene digestion vessel and allowed to incubate for 12 h. The resulting digestion solution was diluted using ultrapure water and stored in a tube until analysis.

2.6.4. Determination of Total Flavonoid Content. The total flavonoid content was determined using the $Al(NO_3)_3$ colorimetric assay conducted by ultraviolet and visible spectrophotometry as described by Huang et al. with minor adjustments [17]. Specifically, 1 mL of each sample and the ruin standard solution were placed into separate tubes containing 1 mL of water. Then, 0.20 mL of 5% $NaNO_2$ was added to the mixture. After a 5-min incubation period, 0.15 mL of 10% $Al(NO_3)_3$ was introduced, and the mixture was left to stand for another 5 min. Following this, 1 mL of 1 mol/L NaOH was added, and the total volume was adjusted to 5 mL with double-distilled water. The solution was thoroughly mixed, and the absorbance was measured at 510 nm using a spectrophotometer reader (Thermo, USA).

2.6.5. Determination of Total Proanthocyanidin Content. The total proanthocyanidin content was assessed using the vanillin–HCl assay with minor adjustments [18]. In brief, 1 mL of each sample and catechin standard solution were placed into tubes. Then, 5 mL of 0.1% vanillin–HCl solution was added and allowed to incubate for 30 min at 30°C before measuring the absorbance at 500 nm using a spectrophotometer reader (Thermo, USA).

2.6.6. Determination of Total Polysaccharide Content. The polysaccharide content was determined using the phenol–sulfuric acid colorimetric method at 485 nm, with minor adjustments [19]. In brief, 1 mL of the diluted polysaccharide sample solution and glucose standard solution were combined with 1.0 mL of 5% phenol and 5 mL of 98% H_2SO_4 and left to stand for 10 min at room temperature. The mixture was then incubated at 40°C for 15 min before measuring the absorbance at 490 nm using a spectrophotometer reader (Thermo, USA).

2.6.7. Determination of Total Dietary Fiber. The total dietary fiber content was determined using the AOAC 991.43 method [20].

3. Results and Discussion

3.1. Chemical Composition of the Raw Petiole Juice. The chemical composition of fresh petiole juice was determined using UPLC–QTOF–MS–MS. The accurate masses and compositions of both precursor and product ions in the fresh petiole juice were analyzed in negative ionization mode.

Ultimately, 36 compounds were tentatively identified, including 5 proanthocyanidins, 16 flavonoids, 9 phenolic acids, and 2 anthraquinones, by comparing their retention behaviors and mass fragmentation characteristics with those reported in previous studies (Table 1). According to the UPLC–QTOF–MS–MS analysis, the petiole juice was found to be particularly rich in phenolic acids, flavonoids, and proanthocyanidins (Figure 1).

Proanthocyanidins, categorized as secondary polyphenol metabolites, were detected in the raw petiole juice. Proanthocyanidin B was selected as a representative for structural elucidation (Figure 2(a)). The primary fragments of proanthocyanidins mainly result from mechanisms such as heterocyclic ring fission, quinone-methide, and retro-Diels–Alder (RDA) fission [21]. The RDA reaction involves a break in the C-ring of flavanols, resulting in the loss of a neutral structure ($C_8H_8O_3$) with a molecular mass of 152. For the B-type proanthocyanidins (Peaks **5**, **6**, and **7**), fragmentation produced ions at m/z 289 and 287. Regarding trimers (Peak **8**), fragments at m/z 577 and 287 were generated through quinone-methide fragmentation in the upper unit. In procyanidin dimers, the ion at m/z 425 underwent the loss of a water molecule, leading to a fragment at m/z 407.

Flavonoids are a class of natural compounds found in plants known for their anti-inflammatory, anticancer, and cardiovascular protective effects. In fresh petiole juice, the aglycones of flavonoids are primarily quercetin. Flavonoid O-glycosides contain multiple phenolic hydroxyl groups in their aglycones, which tend to produce $[M\text{-}H]^-$ ions in the negative ion mode, easily losing sugar chains to form aglycone ions. These ions readily produce C-ring opening ions, such as m/z 255.0525 and 211.0452 fragment ions. Using quercetin–glucopyranoside (**22**) as an example for elucidation, the mass spectrometry fragmentation patterns of flavonoid O-glycosides can be understood (Figure 2(b)).

Anthraquinones found in RT are traditionally used as laxatives. Besides their laxative activities, anthraquinones exhibit antibacterial, antiviral, antifungal, and estrogenic properties. Aloe emodin and emodin glucoside are the main anthraquinone components of rhubarb, and they have also been detected in the petiole. Aloe emodin was selected as a representative for the structural elucidation (Figure 2(c)).

3.2. Network Pharmacology–Based Analysis. In the raw petiole juice of RT, 36 active ingredients were identified, corresponding to 5861 targets after merging and eliminating duplicates. A total of 121 intersection targets were identified by mapping the putative active ingredient targets and disease targets for antidiabetic purposes. A PPI network comprising 121 nodes and 1121 edges was constructed, illustrating the strong correlations among these targets. Following topological analysis of the PPI network, we compiled a list of top-ranking genes, which included TNF, GAPDH, EGFR, SRC, and BCL2.

Among the 36 potential active ingredients, 10 ingredients with higher degrees of interaction were identified as potential major active ingredients in RT raw petiole juice. These include procyanidin C (**8**), catechin–glucoside isomer (**10**), hydroxyrumicin–glucopyranoside (**12**), procyanidin B isomer (**5**), procyanidin B isomer (**6**), procyanidin B isomer (**11**), catechin–glucoside isomer (**7**), diosmetin–glucopyranoside (**28**), procyanidin B -di-O-gallate (**14**), and catechin–glucoside isomer (**4**).

Key targets such as TNF, GAPDH, EGFR, SRC, and BCL2 were pinpointed as vital genes associated with the active compounds of RT petiole juice. Through the topological analysis of the PPI network, these target points have been identified as core nodes. This suggests that the active compounds in the petiole may directly interact with these target points, thereby producing therapeutic effects in the treatment of diabetes [22, 23]. TNF, a crucial proinflammatory mediator, induces insulin resistance through serine phosphorylation, thereby impairing insulin signaling. In addition, TNF is primarily associated with diabetic vascular dysfunction and diabetic nephropathy [24]. GAPDH is a key signaling molecule that regulates insulin metabolism and participates in processes such as glycogen synthesis, glucose uptake, and glucose transport [25]. EGFR plays a role in activating various signaling pathways to translate extracellular signals into appropriate cellular responses. Studies suggest that the correlation between Type 2 diabetes mellitus and ESR1 variants may involve other unidentified ESR1 polymorphisms regulating glucose homeostasis. EGFR is the most extensively investigated factor in diabetic retinopathy [26]. During the advanced stages of diabetic retinopathy, EGFR can facilitate endothelial cell proliferation and contribute to the pathological formation of new blood vessels. PTGS2 negatively regulates glucose-stimulated insulin secretion and acts as a mediator of the inflammatory response associated with decreased insulin sensitivity, potentially mediating susceptibility to Type 2 diabetes mellitus [27]. In summary, the key targets identified are significantly important in diabetes and have been utilized to construct a target interaction network for antidiabetic purposes.

The top 10 terms from the GO analysis and the KEGG metabolic pathways were extracted based on the p value. These targets were primarily involved in biological processes (BPs) such as peptidyl–serine modification, peptidyl–serine phosphorylation, regulation of reactive oxygen species metabolic process, and peptidyl–tyrosine phosphorylation. They were mainly distributed in cellular components such as cytoplasmic vesicle lumen, vesicle lumen, secretory granule lumen, and membrane raft. The molecular functions were predominantly concentrated in calcium-dependent protein kinase C activity, protein kinase C activity, protein serine/threonine kinase activity, and calcium-dependent protein serine/threonine kinase activity (Figure 3). The results of KEGG pathway enrichment analysis indicated that target genes were significantly enriched in pathways including the MAPK signaling pathway, proteoglycans in cancer, Rap1 signaling pathway, AGE–RAGE signaling pathway in diabetic complications, and Ras signaling pathway (Figure 4).

Table 1: Mass spectrometric data of petiole in *R. Tanguticum*.

Peak	t_R (min)	$[M]^-$ (m/z)	Formula	Fragment (m/z)	Tentative identification
1	2.712	331.0662	$C_{13}H_{16}O_{10}$	271.0468, 169.0150	Galloylglucose isomer
2	4.577	331.0668	$C_{13}H_{16}O_{10}$	169.0141	Galloylglucose isomer
3	5.730	331.0681	$C_{13}H_{16}O_{10}$	169.0141	Galloylglucose isomer
4	7.154	451.1245	$C_{21}H_{24}O_{11}$	289.0713, 162.0528	Catechin–glucoside isomer
5	7.629	577.1352	$C_{30}H_{26}O_{12}$	425.0881, 289.0712	Procyanidin B isomer
6	8.239	577.1343	$C_{30}H_{26}O_{12}$	425.0881, 289.0712	Procyanidin B isomer
7	8.916	451.1237	$C_{21}H_{24}O_{11}$	289.0713, 162.0528	Catechin–glucoside isomer
8	9.120	865.1985	$C_{45}H_{38}O_{18}$	425.0922, 289.0728	Procyanidin C
9	9.594	483.0827	$C_{20}H_{20}O_{14}$	169.0135,	Gallic acid (2-O-galloyl) glucoside
10	10.001	451.1244	$C_{21}H_{24}O_{11}$	289.0713	Catechin-glucoside isomer
11	10.306	577.1358	$C_{30}H_{26}O_{12}$	425.0881, 289.0712	Procyanidin B isomer
12	10.612	393.1186	$C_{19}H_{22}O_9$	231.0658	Hydroxyrumicin–glucopyranoside
13	10.951	385.1135	$C_{17}H_{22}O_{10}$	223.0601, 161.0249	Sinapic acid hexoside
14	11.155	881.1621	$C_{44}H_{34}O_{20}$	557.1246	Procyanidin B -di-O-gallate
15	11.663	593.1512	$C_{27}H_{30}O_{15}$	311.0603	Isovitexin-O-glucoside
16	12.375	503.1187	$C_{24}H_{24}O_{12}$	162.0528	Dalpatein 7-O-glucoside
17	12.714	477.1040	$C_{22}H_{22}O_{12}$	301.0358, 109.0297	Coumaroyl-O-galloylglucose
18	12.917	563.1416	$C_{26}H_{28}O_{14}$	477.0960, 275.0617	Apigenin–glucoside–arabinoside isomer
19	13.358	389.1223	$C_{20}H_{22}O_8$	225.0552, 125.0238	Resveratroloside
20	13.730	477.1470	$C_{23}H_{26}O_{11}$	313.0584	Isolindleyin
21	14.477	563.1402	$C_{26}H_{28}O_{14}$	477.0960, 275.0617	Apigenin–glucoside–arabinoside isomer
22	16.002	463.0886	$C_{21}H_{20}O_{12}$	301.0348, 257.0525	Quercetin–glucopyranoside isomer
23	16.409	463.0888	$C_{21}H_{20}O_{12}$	301.0348, 211.0452	Quercetin–glucopyranoside isomer
24	16.680	463.0883	$C_{21}H_{20}O_{12}$	301.0348	Quercetin–glucopyranoside isomer
25	18.307	607.1304	$C_{27}H_{28}O_{16}$	463.0886, 301.0348	Quercetin-O-[3-hydroxy-3-methylglutaryl] hexoside
26	18.376	433.0779	$C_{20}H_{18}O_{11}$	301.0347, 269.0455	Quercetin 3-arabinoside
27	19.054	477.1470	$C_{23}H_{26}O_{11}$	313.0575, 169.0142	Lindleyin
28	20.071	461.1101	$C_{22}H_{22}O_{11}$	299.0565, 269.0454	Diosmetin–glucopyranoside
29	20.781	435.1310	$C_{21}H_{24}O_{10}$	273.0452, 179.0344	Phlorizin
30	22.478	623.1769	$C_{31}H_{28}O_{14}$	315.0503	Isorhamnetin 3-(6″-*p*-coumarylglucoside)
31	22.851	489.1032	$C_{23}H_{22}O_{12}$	301.0343, 285.0392	Quercetin 3-acetyl rhamnoside isomer
32	24.038	489.1051	$C_{23}H_{22}O_{12}$	301.0343	Quercetin 3-acetylrhamnoside isomer
33	25.089	623.1843	$C_{31}H_{28}O_{14}$	459.0962, 163.0399	Hydroxyphenylbutanone (2-galloyl-6-coumaroyl) glucoside
34	25.326	629.1530	$C_{30}H_{30}O_{15}$	465.0708, 313.0574	1,6-Digalloyl-2-O-p-coumaroyl-glucoside
35	25.631	431.0988	$C_{21}H_{20}O_{10}$	269.0507, 179.0348	Emodin–glucoside
36	26.750	269.0455	$C_{15}H_{10}O_5$	253.0507, 121.0285	Aloe emodin

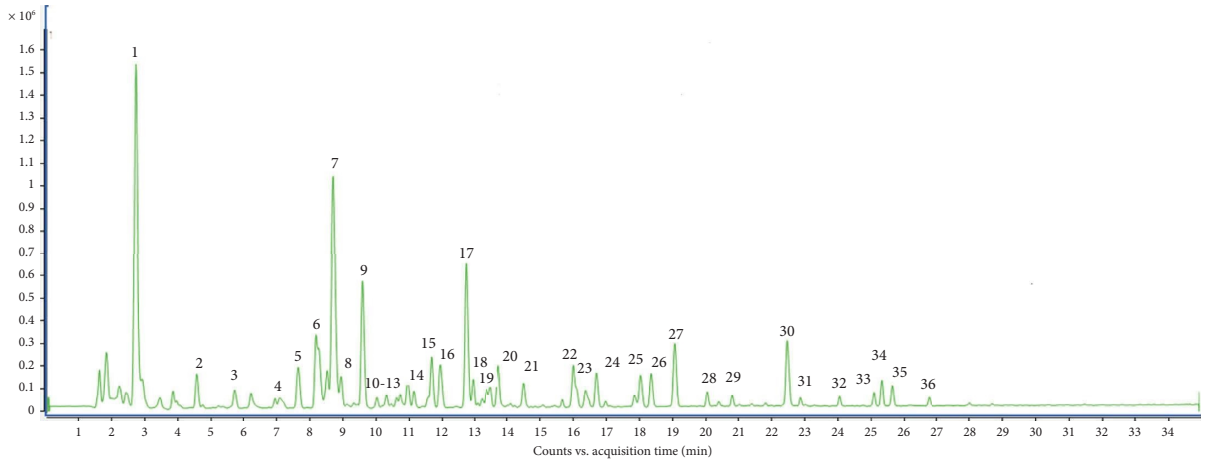


Figure 1: UPLC-QTOF-MS-MS analysis chromatogram of raw petiole juice.

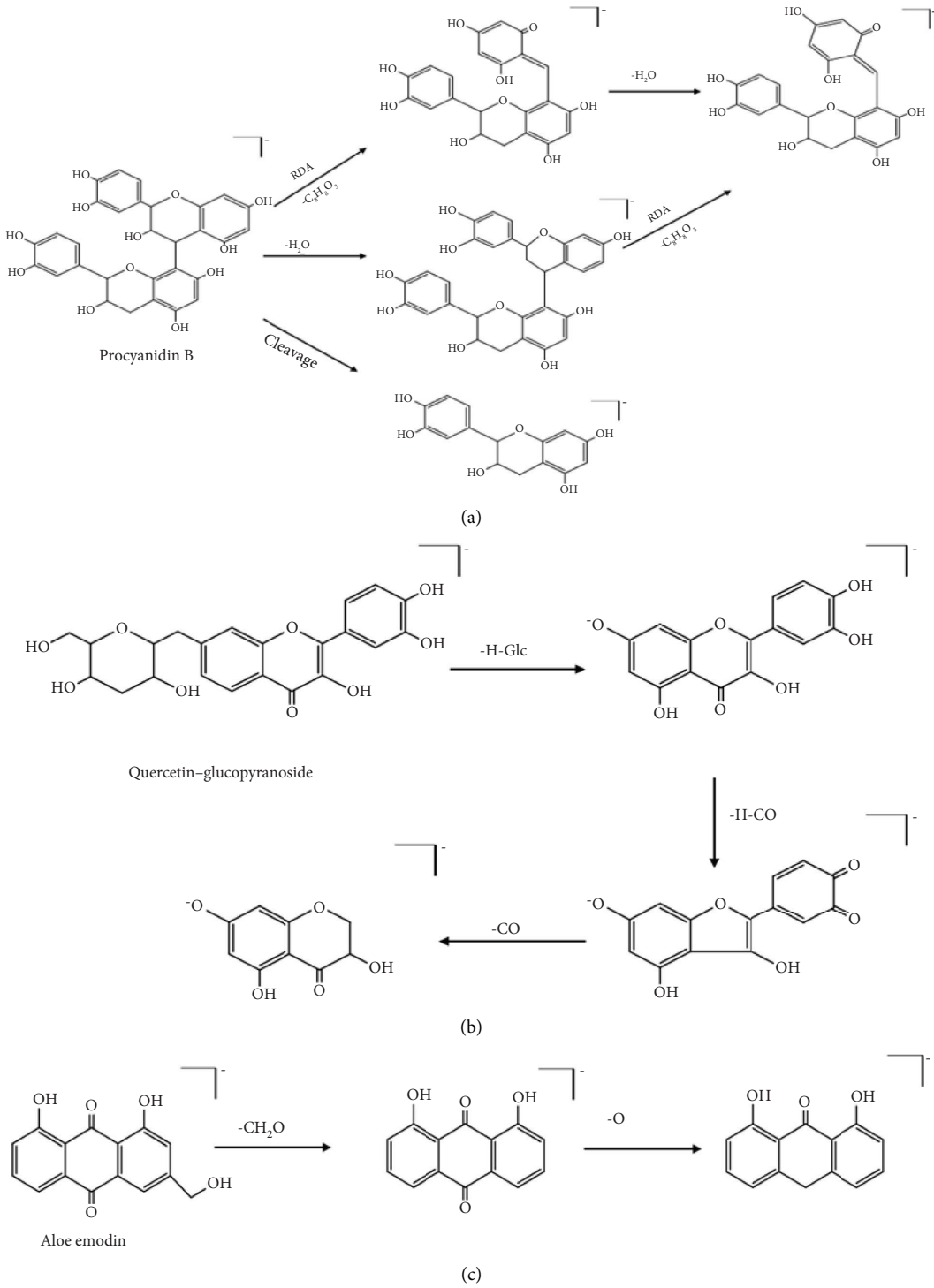


Figure 2: Mass spectrometry fragmentation patterns of proanthocyanidin B (a), quercetin–glucopyranoside (b), and Aloe emodin (c).

The MAPKs are extracellular signal-regulated protein kinases that increase cellular proliferation and regulate cell survival. Previous studies have shown that antidiabetic activity can occur through the MAPK signaling pathway by downregulating p-p38 MAPK, ERK1/2, JNK1, and p-AMPK [28]. MAPKs also govern the inflammatory response alongside a diverse array of cellular processes, including cell metabolism, proliferation, motility, apoptosis, survival, differentiation, and functioning in both physiological and pathological contexts. Prior investigations have indicated that numerous hypoglycemic agents exhibit anti-inflammatory properties, potentially enhancing the management of diabetes and its associated complications [29]. Certain research has suggested that activated Rap1A fosters glucose-stimulated insulin secretion, islet cell hypertrophy, and proliferation, rendering it a distinctive target for

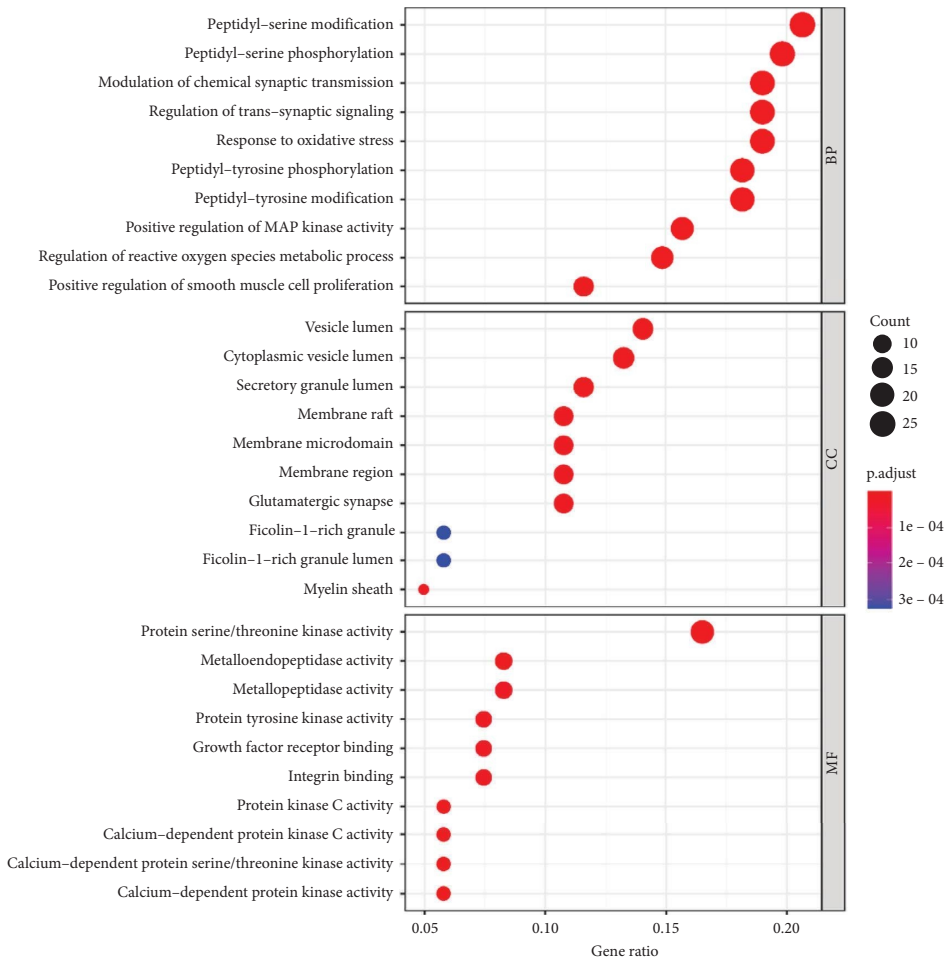


Figure 3: Dot plot of the GO function analysis.

addressing beta-cell dysfunction in diabetes. Furthermore, the signaling pathways associated with Rap1 are implicated in insulin production and the pathophysiology of diabetes [30]. In our current study, it is plausible to assert that RT petiole juice may enhance diabetes treatment by modulating MAPK, Rap1, and other signaling pathways via TNF, GAPDH, and EGFR. These discoveries offer valuable insights, providing a theoretical foundation for addressing diabetes and its associated complications.

To further elucidate the relationship between RT raw petiole juice and its antidiabetic effects, a "compounds–targets–pathways–disease" network was constructed, highlighting the multi-ingredient, multitarget, and multipathway characteristics of traditional Chinese medicine.

3.3. Evaluation of Permeate Flux. Figure 5 illustrates the temporal evolution of flux during the treatment of RT petiole juice using the studied membranes. A typical flux decay was observed, attributed to concentration polarization and contamination phenomena, until steady-state values were reached. The Jp vs. time curve can be divided into two phases: an initial phase characterized by a decrease in flux, and a subsequent phase in which the flux stabilizes. Among the membranes studied, the 0.2 μm membrane exhibited the highest permeate flux, followed by the 0.1 μm and 50 kDa membranes, respectively.

Numerous experiments were conducted using different types of membranes to analyze the behavior of the permeate flux. As depicted in Figure 5, the permeate flux exhibited a gradual decline over operational time across various transmembrane types. Two distinct phases emerged: initially, a notable reduction in permeate flux occurred within the first 100 min across all transmembrane types. Subsequently, the permeate flux experienced a slight further decrease over 200 min of operation until it stabilized at values of 9.52, 9.46, and 7.38 L/m^{2}h for 0.2 μm MF, 0.1 μm MF, and 50 kDa UF, respectively. The subsequent operational phase is widely considered to be a steady-state. Due to the accumulation of juice components in the pores and on the membrane surface, the permeation flux gradually decreases over time until stability is achieved. Similar observations have been reported by other researchers in various membrane studies [31]. Different fouling mechanisms and concentration polarization phenomena, including the convection of feed extractives pushing towards the membrane and facilitating the separation of suspended solids, may all potentially limit flux.

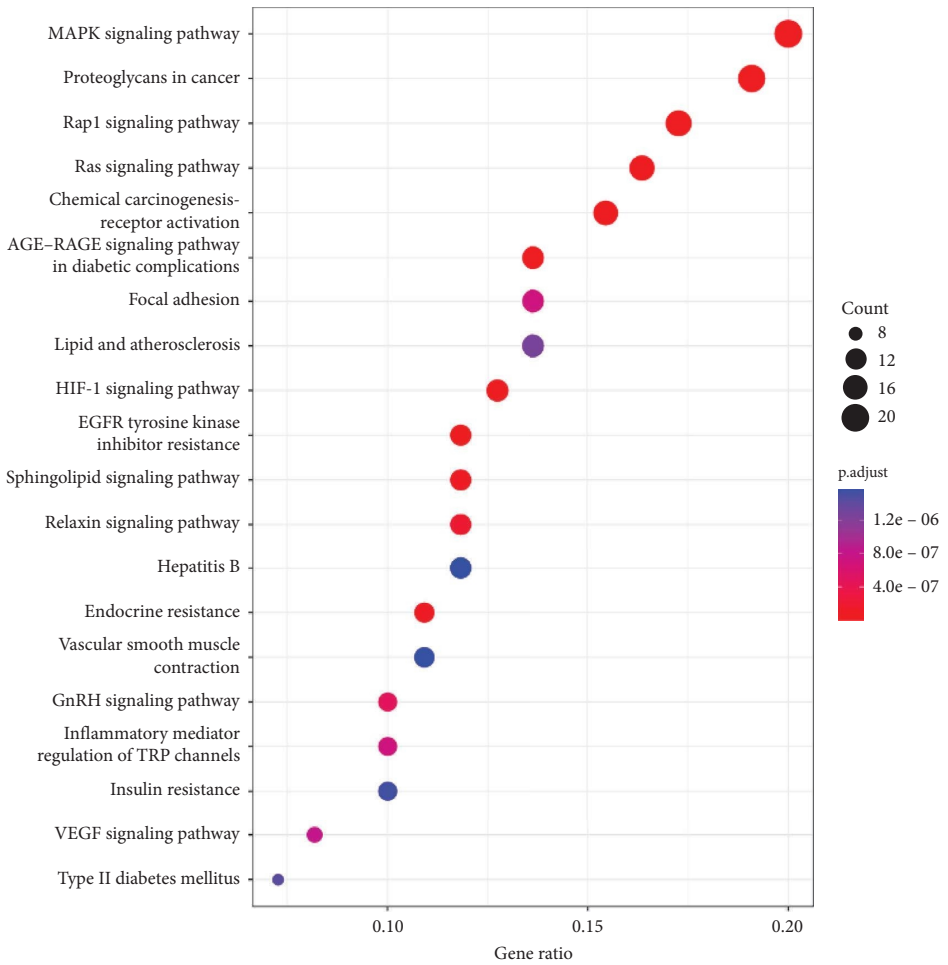


Figure 4: Dot plot of the KEGG pathway enrichment analysis.

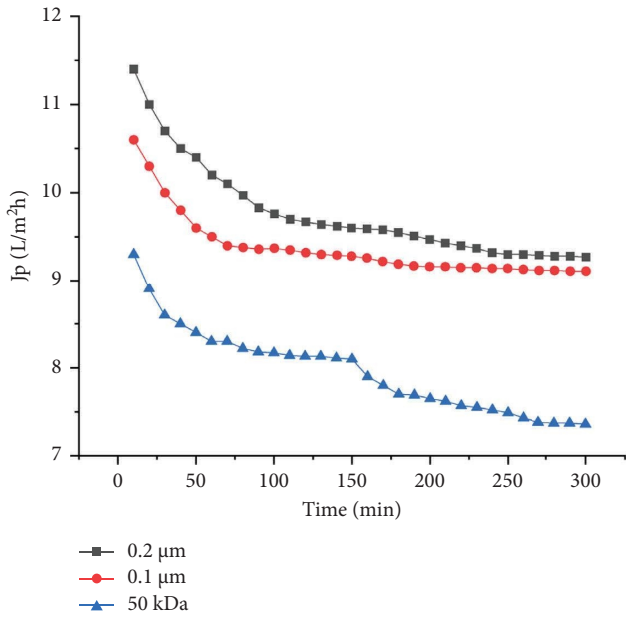


Figure 5: Permeate flux during membrane filtration of juice.

Table 2: Physicochemical properties of the petiole juice before and after the clarification process.

Parameter	Raw juice	0.2 μm MF	0.1 μm MF	50 kDa UF
Total flavonoid (mg/100 g)	0.09[a]	0.04[b]	0.03[b]	0.02[b]
Total polysaccharide (mg/100 mL)	36.21[a]	8.09[b]	7.84[bc]	6.25[cd]
Proanthocyanidins (mg/100 mL)	35.82[a]	8.24[b]	4.93[c]	5.66[c]
Total phenols (mg/L)	754.82[a]	656.02[b]	648.06[b]	632.54[b]
Soluble protein (%)	0.23[a]	0.19[b]	0.16[c]	0.16[c]
Dietary fiber (%)	0.20[a]	0.19[a]	0.18[a]	0.16[a]
Ca (mg/L)	3.13[a]	3.30[a]	4.76[b]	5.23[b]
Al (mg/L)	3.73[a]	2.88[b]	4.21[c]	4.58[c]
Fe (mg/L)	43.63[a]	25.92[b]	35.14[c]	40.17[a]
Mg (g/L)	0.15[a]	0.12[a]	0.15[a]	0.16[a]
K (g/L)	1.73[a]	1.47[a]	1.70[a]	1.73[a]
Mn (mg/L)	1.79[a]	1.40[b]	1.83[a]	1.94[a]
Na (mg/L)	16.5[a]	14.3[a]	17.0[a]	17.6[a]
Zn (mg/L)	0.67[a]	0.52[a]	0.69[a]	0.70[a]

Note: The statistical method we used is one-way ANOVA combined with Tukey's HSD test and marked with letters (a, b, c, etc.); the same letter indicates no significant difference between groups, while different letters indicate a difference at $p < 0.05$.

3.4. Quality of Filtered Juice. Given that membrane processes are nonthermal and entail minimal nutrient loss, they are increasingly utilized in various industrial sectors. Table 2 details the chemical properties of the feed and permeate across different membrane separation processes. No significant differences ($p > 0.05$) were observed in the contents of dietary fiber, Ca, Mg, K, Na, and Zn between juices obtained through different membranes and the raw juice. However, there was a notable decrease in the contents of total flavonoids, total polysaccharides, proanthocyanidins, and total phenols after membrane treatment. After membrane separation, total polysaccharide content levels dropped to 8.09 mg/100 mL with the 0.2 μm MF membrane, 7.84 mg/100 mL with the 0.1 μm MF membrane, and 6.25 mg/100 mL with the 50 kDa UF membrane. Similarly, the proanthocyanidin content in raw juice was 35.82 mg/100 mL, which decreased to 8.24 mg/100 mL, 4.93 mg/100 mL, and 5.66 mg/100 mL after treatment with the 0.2 μm MF, 0.1 μm MF, and 50 kDa UF membranes, respectively. The total phenol content was also reduced from 754.82 mg/L in raw juice to 656.02 mg/L, 648.06 mg/L, and 632.54 mg/L after filtration with the 0.2 μm MF, 0.1 μm MF, and 50 kDa UF membranes, respectively.

Compared to the raw juice, the mineral content in the separated juice both increased and decreased. For example, the Ca content increased from 3.13 mg/L in the raw juice after membrane separation. Conversely, the Fe content decreased from 43.63 mg/L in the raw juice. Similarly, membrane separation had no significant effect on certain mineral elements in the juice, such as K and Zn.

There were no significant differences in total flavonoids, total polysaccharides, total phenols, dietary fiber, and Mg, K, Na, and Zn contents between the 0.1 and 0.2 μm membranes. Except for Fe, other physicochemical properties showed no significant differences between the 0.1 μm MF and 50 kDa UF membranes. Similarly, except for total flavonoids, soluble protein, dietary fiber, Mg, K, Na, and Zn, other physicochemical properties showed significant differences between the 0.2 μm MF and 50 kDa UF membranes.

The juice clarified by the 50 kDa membrane demonstrated the lowest levels of proanthocyanidins, soluble protein, and total polysaccharide content. The trend showed that the level of these components decreased with decreasing membrane pore size. At the beginning of the membrane process, proanthocyanidins, soluble proteins, and total polysaccharides, due to their high molecular weight, are adsorbed onto the membrane pores and surface, preventing them from passing into the permeate. As a result of cake formation, a constant rate of these components passed into the pores, resulting in a stable concentration of these components in the permeate after filtration. In this investigation, the total phenolic content in clarified juice exhibited a decline with decreasing pore size. Phenolic compounds not only face steric hindrance due to their large molecular weight but also cause pore blockage and cake formation. The blocking mechanism typically includes two main interactions: (1) hydrophobic–hydrophobic interaction and (2) benzene ring–benzene ring interaction via π–π stacking [32].

4. Conclusions

In this research, 36 compounds were identified in RT petiole juice using UPLC–QTOF–MS–MS. Network pharmacological analysis revealed five key targets for diabetes treatment: TNF, GAPDH, EGFR, SRC, and BCL2. KEGG pathway enrichment analysis highlighted the importance of several pathways, including the MAPK signaling pathway, PI3K-Akt signaling pathway, proteoglycans in cancer, and the Rap1 signaling pathway. Among all tested membrane types for juice clarification, the best results were achieved with MF membranes with a pore size of 0.2 μm. The juice processed with this membrane exhibited relatively high levels of total flavonoids (0.04 mg/100 g), proanthocyanidins (8.24 mg/100 g), and total phenols (656.02 mg/L) after membrane separation. The type of membrane significantly affected the content of total polysaccharides, proanthocyanidins, soluble protein, Ca, Al, and Fe ($p < 0.05$), but it did not significantly affect the levels of total flavonoids, total phenols, dietary fiber, Mg, K, Mn, Na, or

Zn. Based on these findings, a 0.2 μm membrane is strongly recommended for the MF process of RT petiole juice in industrial applications. This membrane size optimizes the retention of beneficial compounds while ensuring effective juice clarification. The results of this study provide a solid foundation for the industrial processing and utilization of RT petiole juice, highlighting its potential as a functional food ingredient with antidiabetic properties.

Data Availability Statement

The data that support the findings of this study are available from the corresponding author upon reasonable request.

Conflicts of Interest

The authors declare no conflicts of interest.

Author Contributions

Chen Chen: methodology, software, and funding acquisition. Zengrong Ye: writing–reviewing and data curation. Bo Wang: visualization and writing–original draft. Guoying Zhou: supervision and editing. Chen Chen and Zengrong Ye contributed equally to this manuscript.

Funding

This work was supported by the Qinghai Science and Technology Achievement Transformation Project (2021–SF–149).

References

[1] D. Q. Pham, D. T. Ba, N. T. Dao, et al., "Antimicrobial Efficacy of Extracts and Constituents Fractionated From *Rheum Tanguticum* Maxim. Ex Balf. Rhizomes Against Phytopathogenic Fungi and Bacteria," *Industrial Crops and Products* 108 (2017): 442–450, https://doi.org/10.1016/j.indcrop.2017.06.067.

[2] S. A. Pandith, R. A. Dar, S. K. Lattoo, M. A. Shah, and Z. A. Reshi, "*Rheum australe*, an Endangered High-Value Medicinal Herb of North Western Himalayas: A Review of Its Botany, Ethnomedical Uses, Phytochemistry and Pharmacology," *Phytochemistry Reviews* 17, no. 3 (2018): 573–609, https://doi.org/10.1007/s11101-018-9551-7.

[3] T. A. Trinh, D. Lee, S. Park, et al., "Stilbenes Contribute to the Anticancer Effects of *Rheum undulatum* L. Through Activation of Apoptosis," *Oncology Letters* 17, no. 3 (2019): 2953–2959, https://doi.org/10.3892/ol.2019.9926.

[4] L. Xiang, F. Lei, D. Xing, W. Wang, and J. Zheng, "Neuron Protective Constituents From Rheum Nanum and Rheum Sublanceolatum," *Tsinghua Science and Technology* 10, no. 4 (2005): 426–429, https://doi.org/10.1016/s1007-0214(05)70094-8.

[5] C. He, K. Wu, J. Zhang, et al., "Cytochemical Localization of Polysaccharides in *Dendrobium officinale* and the Involvement of DoCSLA6 in the Synthesis of Mannan Polysaccharides," *Frontiers of Plant Science* 8 (2017): 173, https://doi.org/10.3389/fpls.2017.00173.

[6] J. Kolodziejczyk-Czepas and O. Liudvytska, "*Rheum rhaponticum* and *Rheum rhabarbarum*: A Review of Phytochemistry, Biological Activities and Therapeutic Potential," *Phytochemistry Reviews* 20, no. 3 (2021): 589–607, https://doi.org/10.1007/s11101-020-09715-3.

[7] F. Naemi, G. Asghari, H. Yousofi, and H. A. Yousefi, "Chemical Composition of Essential Oil and Anti Trichomonas Activity of Leaf, Stem, and Flower of *Rheum ribes* L. Extracts," *Avicenna journal of phytomedicine* 4, no. 3 (2014): 191–199.

[8] S. M. Son, K. D. Moon, and C. Y. Lee, "Rhubarb Juice as a Natural Antibrowning Agent," *Journal of Food Science* 65, no. 8 (2000): 1288–1289, https://doi.org/10.1111/j.1365-2621.2000.tb10598.x.

[9] R. Tundis, M. R. Loizzo, M. Bonesi, et al., "Concentration of Bioactive Compounds from Elderberry (*Sambucus Nigra* L.) Juice by Nanofiltration Membranes," *Plant Foods for Human Nutrition* 73, no. 4 (2018): 336–343, https://doi.org/10.1007/s11130-018-0686-x.

[10] F. B. Ferreira, F. D. Magalhaes, V. L. Cardoso, and M. H. M. Reis, "Enhanced Conditions to Obtain a Clarified Purple Araca (*Psidium myrtoides*) Fruit Extract," *Journal of Food Process Engineering* 44, no. 1 (2021): e13607, https://doi.org/10.1111/jfpe.13607.

[11] F. H. Li, H. M. Yan, W. Z. Li, J. C. Zhao, and J. Ming, "A Comparative Study of the Effects of Ultrafiltration Membranes and Storage on Phytochemical and Color Properties of Mulberry Juice," *Journal of Food Science* 84, no. 12 (2019): 3565–3572, https://doi.org/10.1111/1750-3841.14935.

[12] F. de Santana Magalhães, M. de Souza Martins Sá, V. Luiz Cardoso, and M. Hespanhol Miranda Reis, "Recovery of Phenolic Compounds From Pequi (*Caryocar brasiliense* Camb.) Fruit Extract by Membrane Filtrations: Comparison of Direct and Sequential Processes," *Journal of Food Engineering* 257 (2019): 26–33, https://doi.org/10.1016/j.jfoodeng.2019.03.025.

[13] D. Pradhan, H. Baishya, and A. B. Das, "Effect of Ultrasound, Centrifugation, and Enzymatic Pretreatments on Phytochemical Properties and Membrane Fouling during Microfiltration of Sohiong (*Prunus nepalensis* L.) Juice," *Food Science and Biotechnology* 31, no. 11 (2022): 1443–1450, https://doi.org/10.1007/s10068-022-01129-5.

[14] M. Wu, S. Qiu, B. Lin, H. Li, and S. Zhang, "Phenolic Components and Biological Activity Analysis of Extracts from Leaves of Different Cultivars of Jaboticaba," *Journal of Southern Argiculture* 53, no. 8 (2022): 2231–2240.

[15] D. Zhu, Y. Zhang, C. Kou, P. Xi, and H. Liu, "Ultrasonic and Other Sterilization Methods on Nutrition and Flavor of Cloudy Apple Juice," *Ultrasonics Sonochemistry* 84 (2022): 105975, https://doi.org/10.1016/j.ultsonch.2022.105975.

[16] C. Chen, Y. Shao, Y. Li, and T. Chen, "Trace Elements in *Lycium barbarum* L. Leaves by Inductively Coupled Plasma Mass Spectrometry after Microwave Assisted Digestion and Multivariate Analysis," *Spectroscopy Letters* 48, no. 10 (2015): 775–780, https://doi.org/10.1080/00387010.2013.856324.

[17] Y. Huang, N. Zhou, P. Tian, et al., "Determination of Total Flavonoids in *Australis Mori* Cortex and *Mori Cortex* of Different Species," *Chinese Wild Plant Resources* 40, no. 6 (2021): 20–24.

[18] J. Yan, Z. Song, Z. Cai, Z. Shen, R. Ma, and M. Yu, "Proanthocyanidin Accumulation in Peach Fruit With Three Types of Flesh Color," *Jiangsu Journal of Agricultural Sciences* 34, no. 3 (2018): 651–656.

[19] S. H. Chen, L. Wu, Y. B. Li, and W. Deng, "Interaction of Plum (*Prunus salicina Lindl.* Cv. Furong) Anthocyanins With Tremella Polysaccharides and Characteristics of Their

Complexes," *Food Science & Technology (Zurich)* 42 (2022): e37322, https://doi.org/10.1590/fst.37322.

[20] B. V. McCleary and C. McLoughlin, "Determination of Insoluble, Soluble, and Total Dietary Fiber in Foods Using a Rapid Integrated Procedure of Enzymatic-Gravimetric-Liquid Chromatography: First Action 2022.01," *Journal of AOAC International* 106, no. 1 (2022): 127–145, https://doi.org/10.1093/jaoacint/qsac098.

[21] L. Gu, M. A. Kelm, J. F. Hammerstone, et al., "Liquid Chromatographic/Electrospray Ionization Mass Spectrometric Studies of Proanthocyanidins in Foods," *Journal of Mass Spectrometry* 38, no. 12 (2003): 1272–1280, https://doi.org/10.1002/jms.541.

[22] K. Kitamura, K. Hayashi, S. Ito, et al., "Effects of SGLT2 Inhibitors on eGFR in Type 2 Diabetic Patients-the Role of Antidiabetic and Antihypertensive Medications," *Hypertension Research* 44, no. 5 (2021): 508–517.

[23] M. Mascaraque, P. Delgado-Wicke, C. Nuevo-Tapioles, et al., "Metformin as an Adjuvant to Photodynamic Therapy in Resistant Basal Cell Carcinoma Cells," *Cancers* 12, no. 3 (2020): 668.

[24] Y. Sun, Y. Zhou, Y. Shi, et al., "Expression of miRNA-29 in Pancreatic β Cells Promotes Inflammation and Diabetes via TRAF3," *Cell Reports* 34, no. 1 (2021): 108576.

[25] J. E. Pessin and A. R. Saltiel, "Signaling Pathways in Insulin Action: Molecular Targets of Insulin Resistance," *Journal of Clinical Investigation* 106, no. 2 (2000): 165–169.

[26] I. Dahlman, M. Vaxillaire, M. Nilsson, et al., "Estrogen Receptor Alpha Gene Variants Associate With Type 2 Diabetes and Fasting Plasma Glucose," *Pharmacogenetics and Genomics* 18, no. 11 (2008): 967–975.

[27] Y. L. Konheim and J. K. Wolford, "Association of a Promoter Variant in the Inducible Cyclooxygenase–2 Gene (PTGS2) With Type 2 Diabetes Mellitus in Pima Indians," *Human Genetics* 113, no. 5 (2003): 377–381.

[28] K. Taniguchi, L. Xia, H. J. Goldberg, et al., "Inhibition of Src Kinase Blocks High Glucose–Induced EGFR Transactivation and Collagen Synthesis in Mesangial Cells and Prevents Diabetic Nephropathy in Mice," *Diabetes* 62, no. 11 (2013): 3874–3886.

[29] H. Yaribeygi, S. L. Atkin, M. Pirro, and A. Sahebkar, "A review of the Anti–Inflammatory Properties of Antidiabetic agents Providing Protective Effects Against Vascular Complications in Diabetes," *Journal of Cellular Physiology* 234, no. 6 (2019): 8286–8294.

[30] P. Martínez, G. Gómez-López, F. García, et al., "RAP1 Protects From Obesity Through Its Extratelomeric Role Regulating Gene Expression," *Cell Reports* 3, no. 6 (2013): 2059–2074.

[31] J. A. A. Mejia and J. Yáñez-Fernandez, "Clarification Processes of Orange Prickly Pear Juice (*Opuntia* spp.) by Microfiltration," *Membranes* 11, no. 5 (2021): 354, https://doi.org/10.3390/membranes11050354.

[32] J. Huang, K. Huang, S. Liu, Q. Luo, and M. Xu, "Adsorption Properties of Tea Polyphenols Onto Three Polymeric Adsorbents With Amide Group," *Journal of Colloid and Interface Science* 315, no. 2 (2007): 407–414, https://doi.org/10.1016/j.jcis.2007.07.005.